UV photochemistry of the L-cystine disulfide bridge in aqueous solution investigated by femtosecond X-ray absorption spectroscopy

Miguel Ochmann[a,†], Jessica Harich[a,†], Rory Ma[b], Antonia Freibert[a,*], Jae Hyuk Lee[b,c], Daewoong Nam[b,c], Sangsoo Kim[b], Intae Eom[b,c], Minseok Kim[b], Yujin Kim[d], Madhusudana Gopannagari[d], Da Hye Hong[d], Briony A. Yorke[e], Tae Kyu Kim[d,*] and Nils Huse[a,*]

[a]*Institute of Nanostructure and Solid State Physics, University of Hamburg and Center for Free-Electron Laser Science, 22761 Hamburg, Germany*

[b]*Pohang Accelerator Laboratory, POSTECH, Pohang 37673, Republic of Korea*

[c]*Photon Science Center, Pohang University of Science and Technology, Pohang 37673, Republic of Korea*

[d]*Department of Chemistry, KAIST , Daejeon 34141, Republic of Korea*

[e]*School of Chemistry, University of Leeds, Leeds, LS2 9JT, United Kingdom*

[†]*equal contribution*

Despite the biological relevance of the disulfide bond as the motive, which stabilizes the tertiary structure of many proteins, its photostability, UV-induced bond cleavage mechanisms and secondary photochemistry are still contested after decades of research. In this study, we employed femtosecond X-ray absorption spectroscopy to unravel the photochemistry of the aliphatic disulfide bridge of the semi-essential proteinogenic amino acid L-cysteine (L-cystine) in aqueous solution. We observe homolytic bond cleavage upon UV irradiation and the emergence of thiyl radicals as the single primary photoproduct and its ultrafast decay due to geminate recombination at remarkably high quantum yield in excess of 80% within 20 ps. These dynamics coincide with the emergence of a secondary product, attributed to the perthiyl radical. More than 70% of broken disulfide bridges form within the first nanosecond after bond cleavage. From these observations, we establish a dynamic photostability of the disulfide bridge and a mechanism of perthiyl radical formation from a 'hot' ground-state parent molecule that asymmetrically fragments along a carbon-sulfur bond, resolving long-standing questions in the photochemistry of disulfide bridges in condensed phase.

Introduction

The disulfide bond moiety plays a key role in the thermal stability of proteins: During protein folding, two L-cysteinyl residues in the amino acid chain can be covalently coupled to form a disulfide bond,[1] either intramolecularly within the same protein monomer[2] or intermolecularly between two protein monomers[3] This disulfide cross-linkage thus stabilizes the tertiary and quaternary structure of proteins. Furthermore, the disulfide bond can act as a radical scavenger, protecting the protein from damage by reactive oxygen and nitrogen species (RONS)[4]. Such reactive species may be generated upon exposure to ultraviolet radiation (UVR) or in response to oxidative stress resulting in redox imbalance[5]. RONS can permanently damage the protein through amino acid oxidation and peptide cleavage, resulting in loss of function and potentially harmful aggregation. In addition, free thiol groups and thioethers from L-cysteine and L-methionine are implicated in radical damage and repair mechanisms.[6,7]

The disulfide UV-photochemistry has been the topic of many studies which have focused on the reactions that may result when breaking S-S or C-S bonds and forming the respective thiyl or perthiyl radicals[8]. The picture emerging from the sum of static and time-resolved studies conducted over a time span of nearly 75 years is

one of a clear distinction between reactions in the gas phase and in solution.

Static and time-resolved studies in the gas phase established that excitation at wavelengths shorter than ~200 nm can break both the C-S and the S-S bond in dimethyl disulfide (DMDS).[9–13] Bookwalter et al. showed the same to be true for low-order di-*n*-alkyl disulfides.[14] With the exception of Rinker et al.[15], excitation at wavelengths longer than ~ 250 nm of various disulfides in the gas phase exclusively leads to thiyl radical formation ranging from the smallest disulfide DMDS to disulfide-containing proteins.[13,14,16–23]. A theoretical study by Luo et al. supports these experiments, finding that population of the two lowest electronically excited states leads to dissociation of the S-S bond.[24] Femtosecond studies of disulfides in the gas-phase have been performed by Stephansen et al.[19,20] (1,2-dithiane) as well as Schnorr et al.[23] (DMDS), both reporting the exclusive formation of thiyl radicals. While the latter study established a thiyl radical formation time of (120 ± 30) fs, Stephansen et al. showed that the bond between the two sulfur atoms (which were connected by a carbon chain) reforms with a time-constant of (2.75 ± 0.23) ps, leading them to suggest an inherent photostability of disulfide bridges in confined spaces.

In solution the photoreactions of disulfides become more complicated. The fission of the S-S bond is the primary reaction reported upon irradiation with wavelengths greater than ~ 250 nm.[8,25–33] Nevertheless, several studies account for the photoproducts of C-S bond scission.[34–41] Notably, these are reported predominantly on tertiary disulfides such as *tert*-butyl disulfide and penicillamine disulfide. However, the temporal resolution of hundreds of nanoseconds or longer do not allow for unequivocally establishing a reaction mechanism.

We have previously demonstrated that time-resolved X-ray absorption spectroscopy (TRXAS) at the sulfur K-edge is a chemically specific tool to observe the UV photochemistry of organosulfur compounds in solution[42,43], allowing the observation that both C-S and S-S bond cleavage are readily accessible at 267 nm excitation within ~70 ps, and that the complete decay of both photoproducts, the thiyl and the perthiyl radicals, occurs on timescales from 0.1 ns up to 150 ns[43]. Previous observations of apparently longer living perthiyl radicals formed from *tert*-disulfides are potentially due to stabilization of sulfur radicals by tertiary carbon substituents attached to the disulfide moiety, significantly prolonging radical life times into the range of microseconds.[27,35,39]

The contradicting results between the isolated molecules and molecules in a condensed phase clearly indicate that further investigation is needed to characterize the role of the disulfide environment on product formation and to clarify the conditions necessary to access a specific photochemical reaction pathway. Reactions subsequent to initial fragmentation such as geminate recombination are in most cases inaccessible in the gas-phase but common in solution[17,44–46] due to the confining forces of a solvent cage or a protein backbone.[47,48] This aspect is of particular importance when considering the role of disulfide photochemistry with respect to protein photostability and function. Previous attempts have been made to mimic disulfide photochemistry occurring in solution or in proteins by investigation of cyclic disulfides in which the terminal biradical geminates are connected by a hydrocarbon chain.[19,49,50] However, several processes that involve an environment acting as a thermodynamic bath and allowing for energy dissipation as well as confinement and escape, are crucially determining factors for disulfide chemistry.

In this study, we investigate the photodissociation dynamics of L-cystine, the disulfide dianion of the amino acid L-cysteine, in aqueous solution upon pulsed UV irradiation with 267 nm light using TRXAS at the sulfur K-edge which lies in the so-called tender X-ray regime (2-5 keV).[51–53] We observe the disulfide

photochemistry on timescales of ~100 fs up to hundreds of picoseconds in aqueous solution, thereby clearly identifying the primary and subsequent reaction steps that allow us to establish photochemical cycles of disulfide photochemistry induced by disulfide bond cleavage.

Results and Discussion

X-ray Absorption Spectra

The static X-ray absorption spectrum of L cystine (**1**) at the sulfur K-edge is shown in Fig. 1A. It exhibits two clearly discernible transitions near 2472 eV that are spaced by about 1.5 eV. At higher energy the beginning of the extended X-ray absorption fine-structure (EXAFS) is visible. Note that we have normalized the absorption spectrum to the sulfur K-edge around which the EXAFS modulation oscillates, as is customary in X-ray spectroscopy. In Fig. 1B differential X-ray absorption spectra are plotted for time delays of 0.3 ps, 3 ps and 10 ps between 267-nm excitation pulses and X-ray probe pulses. Negative signals indicate a loss of absorption ('sample bleaching') and positive signals increased absorption.

At a time delay of 300 fs, a new absorption lineshape has appeared at 2466.9 eV and bleaching can be observed in the region of the lowest sulfur-1s absorption lines of L-cystine. At 3 ps time delay the differential spectrum has partially relaxed to smaller levels. Most distinctly, a shoulder has emerged on the higher energy side of the induced absorption lineshape and the bleach signal exhibits two pronounced minima at energies that coincide with the absorption peaks in Fig. 1A. The broad induced absorption shoulder has fully emerged 10 ps after excitation and the bleach signal clearly resembles a negative replica of the lowest sulfur-1s transitions of L-cystine.

To interpret the spectra in Fig. 1, we have modelled X-ray absorption lines of L-cystine and possible chemical products by time-dependent density functional theory, additional information on computations is provided in the supporting

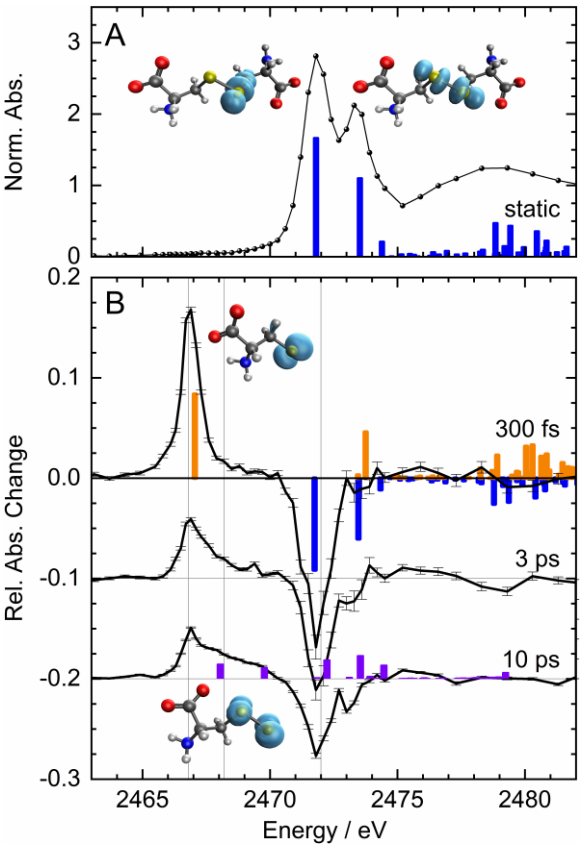

Figure 1: *Static and differential sulfur K-edge absorption spectra of L-cystine with TD-DFT-calculated transitions.* ***A*** *Static spectrum of L-cystine (black) with calculated lowest vertical excitation energies (blue sticks) and corresponding isosurface plots of the difference electron attachment densities (turquoise).* ***B*** *Differential spectra taken 0.3 ps, 3 ps and 10 ps after 267-nm excitation (black). Calculated transitions for the parent ion are shown in blue, for the thiyl radical (**I**) in orange and for the perthiyl radical (**II**) in purple. Isosurface plots (turquoise) show the beta attachment densities of the dominant excitation. The absorption changes are normalized to the K-edge height of L-cystine, i.e. the thiyl radical peak absorption at 300 fs amounts to 17% of the parent molecule's K-edge jump. Vertical grey lines indicate the energies at which delay scans were recorded (c.f. Fig. 3).*

information (SI). The lowest calculated sulfur-1s transitions of L-cystine coincide very well with the experimental transitions in Fig. 1A. We identify these transitions as the excitation of sulfur-1s electrons to sulfur-based π*-orbitals at positions characteristic for aliphatic disulfide bonds. The induced absorption lineshape at 2466.9 eV in Fig. 1B is well described by the lowest sulfur-1s transition of the L-cysteinylthiyl radical (**I**) which has a second transition that overlaps with the second absorption peak of L-cystine (explaining the near lack of a bleach signal at 2473.5 eV). This excellent agreement

between theory and experiment identifies the primary (and only) photoproduct as the two identical thiyl radicals produced from homolytic S–S bond cleavage of L-cystine within 300 fs after 267-nm excitation. This finding establishes that the initial reaction pathways in the gas-phase and in solution are identical. We note that our results are fully consistent with those of Schnorr and co-workers who also established a threshold for two-photon absorption (20 mJ/cm² @ 30-fs excitation)[23] in DMDS that we find for aqueous L-cystine as well (70 mJ/cm² @ 100-fs excitation). At higher peak-power density more than one primary photoproduct will be observed.

The lineshape of the thiyl radical is well described by a Lorentzian, because the energy resolution of the experiment is well below the natural linewidth of sulfur-1s absorption lines. Interestingly, the L-cystine lineshapes in Fig. 1A are inhomogeneously broadened (see lineshape analysis in SI) which we attribute to a distribution of L-cystine conformers that are thermally accessible at room temperature in solution.

The change in differential absorption at time delays of 3 ps and 10 ps clearly indicates a more complex disulfide photochemistry in solution. A secondary product manifests in the form of a broad absorptive shoulder that rises at 2468 eV and higher energy, between the lowest thiyl radical transition and the bleach signal. The 3-ps time delay precludes a diffusive process as the underlying cause for secondary product formation. Thiyl radicals also do not react with water molecules and we can rule out significant formation of solvated electrons in the vicinity of thiyl radicals at our experimental peak-power densities. We therefore consider recombination of the geminate thiyl radicals as the underlying cause for secondary product formation which we identify as the L-cysteineperthiyl radical (**II**). Firstly, theory provides the best match between the lowest absorptive transitions of perthiyl radicals and additional experimental absorption changes at picosecond time delays. Secondly, the bond dissociation energy (BDE) of the

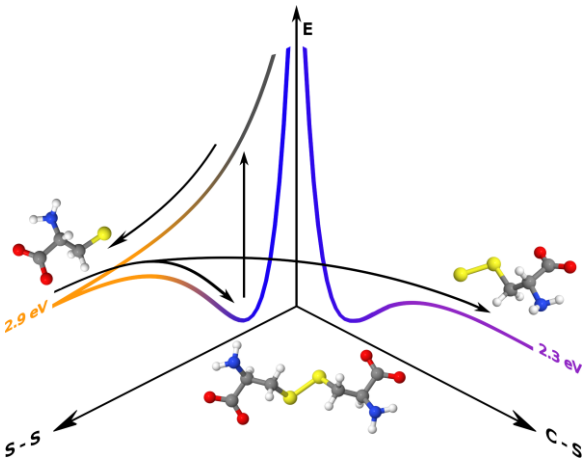

Figure 2: *Schematic of the proposed initial and secondary reaction pathways. After photoexcitation (vertical arrow), the L-cystine molecule splits homolytically into two identical thiyl radicals. Geminate recombination of these thiyl radicals occurs at a $BDE_{S\text{-}S}$ = 2.9 eV[51], energetically high enough for C-S bond cleavage at a $BDE_{C\text{-}S}$ = 2.3 eV[52] (horizontal curved arrow). Alternatively, the parent ground state molecule is reformed by intra- and intermolecular energy relaxation (down-curved arrow toward energy minimum).*

carbon-sulfur bond is about 20% lower than the one of the S-S bond, making this reaction pathways energetically accessible. Lastly, other chemical species are energetically much less likely as we discuss in the SI.

The proposed secondary reaction pathway upon geminate recombination is illustrated in Fig. 2. UV-excitation at 267-nm wavelength (4.6 eV) populates an antibonding state in disulfides (vertical arrow) which must feature an energy barrier of ~6.2 eV (200 nm wavelength) along the C-S bond because only S-S bond cleavage has been reported in the literature for excitation energies below ~6.2 eV. The thiyl radicals are formed at a bond energy of 2.9 eV, [54] the minimum energy at which. geminate recombination occurs with respect to the ground-state energy of L-cystine, thereby providing energy in access of the C-S bond dissociation energy of 2.3 eV. [55] If the time-scale of C-S bond cleavage is on the order of or shorter than relaxation of electronic energy to vibrational energy, perthiyl formation is energetically well possible.

Temporal product evolution

The spectral evolution of the differential sulfur

K-edge absorption already reveals the essentials of the earliest L-cystine photochemistry in aqueous solution. However, we can quantify chemical reaction rates and yields by following the time evolution of the absorption changes at characteristic spectral positions. We probed the absorption changes at the three energies indicated in Fig. 1 by grey vertical lines which are proportional to the concentration of the primary and secondary photoproducts as well as the loss of the parent compound.

The transients are plotted in Fig. 3. The bleach signal at 2472.0 eV (blue) emerges within our time resolution of 200 fs and decays on multiple timescales. About half the signal vanishes within the first 2 ps, and about a quarter of the signal persists much longer than the largest time delay of 0.8 ns. The induced absorption at 2466.8 eV (orange), associated with the primary photoproduct, qualitatively appears to be the mirror image of the bleach transient, decaying within the first 2 ps by more than half and also exhibiting a persistent signal at 0.8 ns time delay. The induced absorption that we associate with the secondary photoproduct was probed at 2468.2 eV (purple). The initial signal rise within the first few hundred femtoseconds can be clearly seen in the inset of Fig. 3. This induced absorption continues to rise substantially within the first 2 ps and more slowly up to tens of picoseconds before it partially decays on hundreds of picoseconds with a persistent signal at the longest time delay of 0.8 ns.

We note three key observations that motivate our kinetic model: Firstly, we observe a signal relaxation at the energy positions that we associate with the primary photoproduct and parent molecule bleaching within the first 2 ps and the first 20 ps. Secondly, the signal at the probe energy associated with the secondary photoproduct rises on these two timescales. Thirdly, the signal at 2466.8 eV appears to be constant between 20 ps and 0.8 ns while the transients at 2468.2 eV and at 2472.0 eV decay slightly in this time interval.

We have employed a rate-equation model to

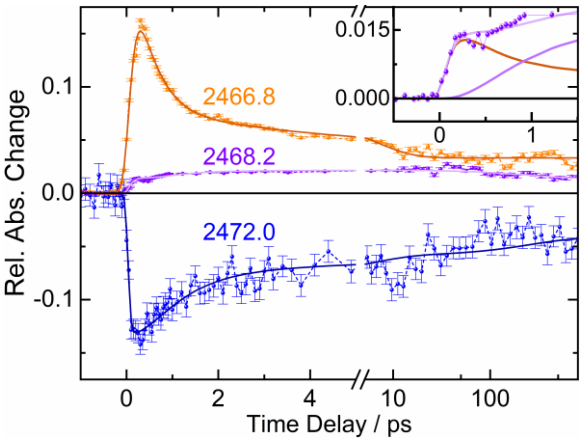

***Figure 3**: Delay scans at the three indicated spectral positions along with fits of a rate-equation model according to Scheme 1. The induced absorption at 2466.8 eV we associate with the L-cysteinylthiyl radical (**I**, orange). The induced absorption at 2468.2 eV is attributed to the L-cysteinylperthiyl radical (**II**, purple). The inset shows this data around zero delay. The spectral position contains 8% contributions from **I** as derived by a Lorentzian lineshape analysis (see Table S1). The bleach signal at 2472.0 eV we attribute to a transient loss of L-cystine (**1**, blue).*

describe the data in Fig. 3. Importantly, the multiple timescales suggest that at least three different sub-ensembles exist that can be associated with the three timescales on which we see signals changes, i.e. 2 ps, 20 ps and much longer timescales. In this model, thiyl radicals either geminately recombines within 2 ps, within 20 ps, or not at all within our observation window of 0.8 ns. This model can be rationalized physically in the following way: The majority of thiyl radicals geminately recombines very rapidly within 2 ps. Because of the fluctuating solvent environment some thiyl radical pairs will rotate substantially during dissociation which will require rotational diffusion for geminate recombination, the timescale of which aligns very well with the 20-ps range we observe. Some fraction of radical pairs escapes the solvent cage and their recombination will take place on diffusive timescales that are beyond the sub-nanosecond timescale that we have probed.

We have summarized the result of our kinetic modelling in Scheme 1 with the exponential time constants for radical formation (τ_1), geminate recombination (τ_{2i}), energy relaxation/perthiyl formation (τ_{3i}), and C-S bond reformation (τ_{4i}). We find a thiyl radical formation time of

(140±50) fs which aligns very well with the 120 fs that Schnorr and co-workers find for gas-phase DMDS.[23] Remarkably, dominant S-S bond reformation with a quantum yield of $\phi_{21} = 0.67$ is ultrafast with a time-constant of $\tau_{21} = 410$ fs, making it an order of magnitude faster than what gas-phase experiments have observed for 1,2-dithiane.[19,20] The capability of ultrafast geminate recombination highlights the importance of confinement and energy dissipation in condensed phases. The additional decay of the thiyl radical signal manifests in a second decay constant of $\tau_{22} = 5.7$ ps at a quantum yield of $\phi_{41} = 0.19$. This means that five out of six thiyl radical pairs recombine within 20 ps.

Our model also provides a relative yield of $\phi_{32} = 0.34$ for secondary product formation, i.e. every third recombination of two thiyl radicals leads to C-S bond cleavage. Almost half of the perthiyl radicals recombine in less than a nanosecond (with a relative yield of $\phi_{41} = 0.42$ and a time constant of $\tau_{41} = 270$ ps). In sum, 70% of dissociated L-cystine molecules have recombined within 1 ns. Because our maximum time delay is 0.8 ns, we estimate that longer-lived radical products must have time constants larger than 10 ns. Table 1 contains the relative yields and time constants extracted from fitting the kinetic model to the delay scans in Fig. 3.

Table 1: *Optimized global fit parameters of the kinetic model employed.*

time constants	relative yields
$\tau_1/\mathrm{ps} = 0.14 \pm 0.02$	
$\tau_{21}/\mathrm{ps} = 0.41 \pm 0.05$	$q_{21} = 0.67 \pm 0.02$
$\tau_{22}/\mathrm{ps} = 5.66 \pm 0.51$	$q_{22} = 0.19 \pm 0.01$
$\tau_{31}/\mathrm{ps} = 0.63 \pm 0.26$	$q_{31} = 0.66 \pm 0.04$
$\tau_{32}/\mathrm{ps} = 0.45 \pm 0.06$	$1 - q_{31}$
$\tau_{41}/\mathrm{ps} = 268 \pm 165$	$q_{41} = 0.42 \pm 0.11$

The high yield with which the S-S bond in aliphatic disulfide reforms on ultrafast timescales upon homolytic bond cleavage suggests that the charge density of the thiyl

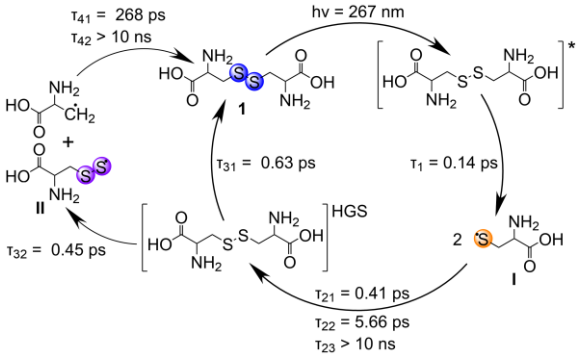

Scheme 1: *Photochemical cycles proposed for UV-excited L-cystine (**1**) in aqueous solution. Upon illumination with a 267-nm light, the S-S bond in **1** is cleaved symmetrically yielding two L-cysteinylthiyl radicals (**I**). Geminate recombination facilitates C-S bond cleavage to form the L-cysteinylperthiyl radical (**II**) as a secondary reaction from the parent 'hot' ground state (HGS). Alternatively, **1** is reformed by intramolecular energy relaxation or by recombination of the perthiyl and carbonyl radicals.*

radicals does not relax substantially but allows for facile bond formation and vibrational energy dissipation such that the high-energy quantum of the UV photon, that was initially absorbed, can be dissipated effectively by bond cleavage and geminate recombination. The photocycles of disulfide chemistry in the condensed phase may therefore have little consequence for the structural integrity of disulfide-stabilized proteins, due to a dynamical photostability of the aliphatic disulfide bond motif.

Conclusions

We have elucidated the UV photochemistry of the L-cystine upon 267-nm excitation by employing femtosecond X-ray absorption spectroscopy at the sulfur K-Edge. Solvent mediated primary geminate recombination occurs effectively, forming a hot ground state, which can lead to perthiyl radical formation, albeit in minority yield. This in turn underscores the very effective radical quenching ability of thiyl radicals via radical recombination, further underlining the potential importance of sulfur functional groups in radical quenching reactions in proteins.

More generally, X-ray absorption spectroscopy at the sulfur K-edge is a valuable tool to gain information about the UV photochemistry of organosulfur compounds, in

the condensed phase, suggestion further the applications in biologically relevant settings, for instance in proteins, where backbone motion plays a role for the recombination probability of thiyl radicals.[56] In summary, we clarified that only homolytic bond cleavage of the disulfide bond occurs upon UV excitation below 6.2 eV (>200 nm wavelength), generating exclusively thiyl radicals as primary photoproducts. Furthermore, we suggest a mechanism for the generation of perthiyl radicals in solution in a secondary reaction step with relatively low yield, thereby providing a possible answer to a long-standing discussion. It will be very interesting to follow disulfide photochemistry in proteins where, in conjunction with aromatic residues, additional reaction pathways such as charge and energy transfer will influence photo-driven disulfide chemistry.

Methods

Experimental Setup

All measurements were conducted at the NCI beamline of the PAL-XFEL free electron laser, Republic of Korea. The setup has been described in detail elsewhere.[57–59] Briefly, the sample was excited with the third harmonic (267 nm) of a Ti:Sa amplified laser system at 60 Hz repetition rate and 100 fs pulse duration (FWHM) of the UV pulses. The round laser focus diameter was 145 µm (1/e^2). For differential XAS spectra and transients a power density of 0.75 TW/cm² was used. Assuming an X-ray pulse width of $\sigma_{X-ray} = \sim 20$ fs, a laser pulse width of $\sigma_{laser} = \sim 45$ fs, a broadening from the sample due to the group velocity dispersion of ~ 65 fs and a temporal jitter between X-rays and laser of 10 fs, the total expected width of the instrument response function (IRF) would be $\sigma_{IRF} = \sim 82$ fs. The X-rays were delivered in a pulse train of 30 Hz and X-ray absorption and changes thereof were detected in fluorescence mode by an avalanche photodiode (APD) shielded with an aluminum foil (thickness: 1.6 µm). The X-rays are focused to 14 x 15 µm² at the sample position. The energies of the X-rays were shifted by + 0.1 eV according to our calibration, which takes several X-ray sources into account (see Supporting Information of Ochmann et al.[43]). The sample was delivered through a 150-µm round steel nozzle into a vacuum chamber at 1 atm pressure of helium.

Materials

L-cystine (99.7 % TLC) and sodium hydroxide (BioXtra, ≥ 98 %) were purchased from Sigma-Aldrich Republic of Korea and were used as received without further purification. In total 200 mL of an aqueous solution containing 4.80 g L-cystine (100 mM) and 2.39 g NaOH (300 mM) were prepared. Half of the sample solution was loaded into the jet's sample reservoir for measurements. After 5 hours of running in a continuous loop, the sample was replaced with the remaining fresh sample solution. No change in X-ray absorption of the unexcited sample was observed during the measurement intervals.

Kinetic Modelling

We have modelled transient delay scans at three characteristic spectral positions by the solution of a rate-equation model convolved with Gaussian instrument response function, where the $N_{ij}(t)$ are the time-dependent partial populations with N_1 as the excited-state population, N_2 as the population of **I**, N_3 as the population of the 'hot' ground-state (HGS) parent molecule, N_4 as the population of **II** and N_0 as the population of **1**. The populations of N_2, N_3, and N_4 are a sum of sub-ensembles to account for multiple relaxation timescales as observed in the experiment. Here, $k_{ij} = 1/t_{ij}$ are the rate constants of the corresponding population decay and q_{ij} are the relative populations of the sub-ensemble on which a rate constant is applied:

$$N_1'(t) = -k_1 N_1(t)$$

$$\dot{N}_2(t) = k_1 N_1(t) - \sum_{i=1}^{3} q_{2i}\, k_{2i} N_{2i}(t)$$

$$\dot{N}_3(t) = \sum_{i=1}^{2} q_{2i} k_{2i} N_{2i}(t) - \sum_{i=1}^{3} q_{2i} \sum_{j=1}^{2} q_{3j}\, k_{3j} N_{3j}(t)$$

$$\dot{N}_4(t) = \sum_{i=1}^{3} q_{2i}\, q_{32} k_{32} N_{32}(t) - \sum_{i=1}^{3} q_{2i} \sum_{j=1}^{2} q_{3j} \sum_{i=1}^{2} q_{4i}\, k_{4i} N_{4i}(t)$$

$$\dot{N}_0(t) = \sum_{i=1}^{3} q_{2i}\, q_{31} k_{31} N_{31}(t) + \sum_{i=1}^{3} q_{2i} \sum_{j=1}^{2} q_{3j}\, q_{41} k_{41} N_{41}(t)$$

$$N_1(0) = 1, N_2(0) = N_3(0) = N_0(0) = 0$$

In the Supporting Information a detailed solution for the differential equation system is given and a schematic representation of the proposed reaction scheme is shown in the Supporting Information Figure S3. Within this model the first state N_1 and the HGS N_3 are not observed with our method. N_1 is assumed to feed into the first state observed, N_2. N_2 then feeds into the dark HGS N_3.The modelled time constant corresponding to the mentioned dark state is below the experiment's time resolution at τ_1 = 0.14 ps. The modelled width σ_{IRF} of the instrument response function (IRF), assuming a Gaussian shape, was fit as $\sigma_{IRF} = (87 \pm 6)$ fs, giving an experimental time resolution of about 200 fs full width at half maximum (FWHM). This agrees with the experimental IRF width. The transients were fit with global time constants $\left\{\tau_{ij}^{\text{global}}\right\}, ij = 01, 21, 22, 31, 32, 41$ where the time constants have been fit simultaneously to all three transients.

Theory Calculations

Equilibrium structure optimizations of all molecular species were performed at the second order Møller-Plesset perturbation theory[60] (MP2) using the Dunning correlation consistent basis set[61] aug-cc-pvtz, where vibrational frequency calculations confirmed the finding of true energetic minima. Ground state calculations were carried out using the quantum chemistry software package Gaussian.[62]

The X-ray absorption transitions were simulated using time-dependent density functional theory (TD-DFT) at the level of the PBE0/def2-TZVP(-f) functional[63,64] using the RIJCOSX approximation. The conductor-like polarizable continuum model using water as solvent model was applied, too. The transition energies of all calculated species were shifted by 52.09 eV to match the experimental spectra. All X-ray transition properties were calculated using the quantum chemistry program Orca[65,66].

Data availability

The data that support the findings of this study are available from the corresponding authors upon reasonable request.

References

1. Creighton, T. E. Disulphide bonds and protein stability. *BioEssays* **8**, 57–63 (1988).
2. Chen, W. *et al.* Intramolecular Disulfide Bond between Catalytic Cysteines in an Intein Precursor. *J. Am. Chem. Soc.* **134**, 2500–2503 (2012).
3. Welker, E., Raymond, L., Scheraga, H. & Caughey, B. Intramolecular Versus Intermolecular Disulfide Bonds in Prion Proteins. *J. Biol. Chem.* **277**, 33477–81 (2002).
4. Halliwell, B. & Gutteridge, J. M. *Free Radicals in Biology and Medicine*. (Oxford university press, USA, 2015).
5. Winterbourn, C. C. Hydrogen peroxide reactivity and specificity in thiol-based cell signalling. *Biochem. Soc. Trans.* **48**, 745–754 (2020).
6. Costa, V., Quintanilha, A. & Moradas-Ferreira, P. Protein oxidation, repair mechanisms and proteolysis in Saccharomyces cerevisiae. *IUBMB Life* **59**, 293–298 (2007).
7. Ezraty, B., Gennaris, A., Barras, F. & Collet, J.-F. Oxidative stress, protein damage and repair in bacteria. *Nat. Rev. Microbiol.* **15**, 385–396 (2017).
8. Lyons, W. E. Photolysis of organic disulphides. *Nature* **162**, 1004–1004 (1948).

9. Callear, A. B., Connor, J. & Dickson, D. R. Electronic spectra of thioformaldehyde and the methyl thiyl radical. *Nature* **221**, 1238–1238 (1969).
10. Callear, A. B. & Dickson, D. R. Transient spectra and primary processes in the flash photolysis of CH 3 SSCH 3, CH 3 SCH 3, CH 3 SH and C 2 H 5 SH. *Trans. Faraday Soc.* **66**, 1987–1995 (1970).
11. Ohbayashi, K., Akimoto, H. & Tanaka, I. Emission spectrum of CH3S radical. *Chem. Phys. Lett.* **52**, 47–49 (1977).
12. Nourbakhsh, S., Liao, C.-L. & Ng, C. Y. A 193 nm laser photofragmentation time-of-flight mass spectrometric study of CH3SSCH3, SSCH3, and SCH3. *J. Chem. Phys.* **92**, 6587–6593 (1990).
13. Lee, Y. R., Chiu, C. L. & Lin, S. M. Ultraviolet photodissociation study of CH3SCH3 and CH3SSCH3. *J. Chem. Phys.* **100**, 7376–7384 (1994).
14. Bookwalter, C. W., Zoller, D. L., Ross, P. L. & Johnston, M. V. Bond-selective photodissociation of aliphatic disulfides. *J. Am. Soc. Mass Spectrom.* **6**, 872–876 (1995).
15. Rinker, A., Halleman, C. D. & Wedlock, M. R. Photodissociation dynamics of dimethyl disulfide. *Chem. Phys. Lett.* **414**, 505–508 (2005).
16. Rao, P. M. & Knight, A. R. Reactions of thiyl radicals. V. The gas phase photolysis of methyl disulfide and ethyl disulfide mixtures in the presence of ethylene. *Can. J. Chem.* **46**, 2462–2464 (1968).
17. Kumar, A., Chowdhury, P. K., Rama Rao, K. V. S. & Mittal, J. P. Four-centered concerted ethane elimination in the IR and UV laser photolysis of dimethyldisulfide. Real-time observation of S2 and CH3S radicals. *Chem. Phys. Lett.* **198**, 406–412 (1992).
18. Agarwal, A., Diedrich, J. K. & Julian, R. R. Direct elucidation of disulfide bond partners using ultraviolet photodissociation mass spectrometry. *Anal. Chem.* **83**, 6455–6458 (2011).
19. Stephansen, A. B. *et al.* Surprising intrinsic photostability of the disulfide bridge common in proteins. *J. Am. Chem. Soc.* **134**, 20279–20281 (2012).
20. Stephansen, A. B., Larsen, M. A. B., Klein, Liv. B. & Sølling, T. I. On the photostability of the disulfide bond: An electronic or a structural property? *Chem. Phys.* **442**, 77–80 (2014).
21. Harrison, A. W., Ryazanov, M., Sullivan, E. N. & Neumark, D. M. Photodissociation dynamics of the methyl perthiyl radical at 248 and 193 nm using fast-beam photofragment translational spectroscopy. *J. Chem. Phys.* **145**, 024305 (2016).
22. Wongkongkathep, P. *et al.* Enhancing protein disulfide bond cleavage by UV excitation and electron capture dissociation for top-down mass spectrometry. *Int. J. Mass Spectrom.* **390**, 137–145 (2015).
23. Schnorr, K. *et al.* Tracing the 267 nm-Induced Radical Formation in Dimethyl Disulfide Using Time-Resolved X-ray Absorption Spectroscopy. *J. Phys. Chem. Lett.* **10**, 1382–1387 (2019).
24. Luo, C., Du, W.-N., Duan, X.-M., Liu, J.-Y. & Li, Z.-S. Theoretical study on the excited states and photodissociation mechanism of dimethyldisulfide. *Chem. Phys. Lett.* **469**, 242–246 (2009).
25. Smissman, E. E. & Sorenson, J. R. The electron spin resonance spectra of disulfides irradiated with ultraviolet light. *J. Org. Chem.* **30**, 4008–4010 (1965).
26. Sayamol, K. & Knight, A. R. Reactions of thiyl radicals. III. Photochemical equilibrium in the photolysis of liquid disulfide mixtures. *Can. J. Chem.* **46**, 999–1003 (1968).
27. Ito, O. & Matsuda, M. Flash photolysis study on the addition reaction of alkylthiyl radical to olefins. *Bull. Chem. Soc. Jpn.* **51**, 427–430 (1978).
28. Gupta, D. & Knight, A. R. Reactions of thiyl radicals. XIII. Photochemically induced

exchange reactions of liquid alkyl disulfides. *Can. J. Chem.* **58**, 1350–1354 (1980).
29. Barrón, L. B. *et al.* Mechanism and kinetics of photoisomerization of a cyclic disulfide, trans-4, 5-dihydroxy-1, 2-dithiacyclohexane. *J. Phys. Chem. A* **108**, 2247–2255 (2004).
30. Kolano, C., Helbing, J., Bucher, G., Sander, W. & Hamm, P. Intramolecular disulfide bridges as a phototrigger to monitor the dynamics of small cyclic peptides. *J. Phys. Chem. B* **111**, 11297–11302 (2007).
31. Mozziconacci, O., Sharov, V., Williams, T. D., Kerwin, B. A. & Schöneich, C. Peptide cysteine thiyl radicals abstract hydrogen atoms from surrounding amino acids: the photolysis of a cystine containing model peptide. *J. Phys. Chem. B* **112**, 9250–9257 (2008).
32. Mozziconacci, O., Kerwin, B. A. & Schöneich, C. Photolysis of an intrachain peptide disulfide bond: primary and secondary processes, formation of H2S, and hydrogen transfer reactions. *J. Phys. Chem. B* **114**, 3668–3688 (2010).
33. Engel, P. S., Gudimetla, V. B., Gancheff, J. S. & Denis, P. A. Solution phase photolysis of 1, 2-dithiane alone and with single-walled carbon nanotubes. *J. Phys. Chem. A* **116**, 8345–8351 (2012).
34. Rosenfeld, S. M., Lawler, R. G. & Ward, H. R. Photo-CIDNP [chemically induced dynamic nuclear polarization] from carbon-sulfur cleavage of alkyl disulfides. *J. Am. Chem. Soc.* **94**, 9255–9256 (1972).
35. Morine, G. H. & Kuntz, R. R. Observations of C-S and S-S bond cleavage in the photolysis of disulfides in solution. *Photochem. Photobiol.* **33**, 1–5 (1981).
36. Joshi, A. & Yang, G. C. Spin trapping of radicals generated in the UV photolysis of alkyl disulfides. *J. Org. Chem.* **46**, 3736–3738 (1981).
37. Grant, D. W. & Stewart, J. H. THE PHOTOLYSIS OF PENICILLAMINE DISULPHIDE INWATER–2-PROPANOL SOLUTIONS. *Photochem. Photobiol.* **41**, 621–623 (1985).
38. Burkey, T. J. *et al.* The tert-butylperthiyl radical. *J. Org. Chem.* **50**, 4966–4967 (1985).
39. Everett, S. A., Schoeneich, C., Stewart, J. H. & Asmus, K. D. Perthiyl radicals, trisulfide radical ions, and sulfate formation: A combined photolysis and radiolysis study on redox processes with organic di-and trisulfides. *J. Phys. Chem.* **96**, 306–314 (1992).
40. Creed, D. The Photophysics and Photochemistry of the Near-Uv Absorbing Amino Acids-Iii. Cystine and Its Simple Derivatives. *Photochem. Photobiol.* **39**, 577–583 (1984).
41. Ramakrishnan, V., Thompson, S. d. & McGlynn, S. P. Photolysis of Some Cyclic Disulfides*. *Photochem. Photobiol.* **4**, 907–915 (1965).
42. Ochmann, M. *et al.* Light-Induced Radical Formation and Isomerization of an Aromatic Thiol in Solution Followed by Time-Resolved X-ray Absorption Spectroscopy at the Sulfur K-Edge. *J. Am. Chem. Soc.* **139**, 4797–4804 (2017).
43. Ochmann, M. *et al.* UV-Photochemistry of the Disulfide Bond: Evolution of Early Photoproducts from Picosecond X-ray Absorption Spectroscopy at the Sulfur K-Edge. *J. Am. Chem. Soc.* **140**, 6554–6561 (2018).
44. Hirata, Y., Niga, Y., Makita, S. & Okada, T. Geminate Recombination of the p-Aminophenylthiyl Radical Pair Produced by the Photodissociation of p-Aminophenyl Disulfide in Nonpolar Solvents. *J. Phys. Chem. A* **101**, 561–565 (1997).
45. Ernsting, N. P. Solvation of photolytically generated p-aminophenylthiyl radicals studied by sub-picosecond transient absorption. *Chem. Phys. Lett.* **166**, 221–226 (1990).
46. Bultmann, T. & Ernsting, N. P. Competition between geminate recombination and

solvation of polar radicals following ultrafast photodissociation of bis (p-aminophenyl) disulfide. *J. Phys. Chem.* **100**, 19417–19424 (1996).
47. Franck, J. & Rabinowitsch, E. Some remarks about free radicals and the photochemistry of solutions. *Trans. Faraday Soc.* **30**, 120–130 (1934).
48. Rabinowitch, E. & Wood, W. C. The collison mechanism and the primary photochemical process in solutions. *Trans. Faraday Soc.* **32**, 1381–1387 (1936).
49. Rankine, C. D., Nunes, J. P. F., Robinson, M. S., Lane, P. D. & Wann, D. A. A theoretical investigation of internal conversion in 1, 2-dithiane using non-adiabatic multiconfigurational molecular dynamics. *Phys. Chem. Chem. Phys.* **18**, 27170–27174 (2016).
50. Middleton, C., D. Rankine, C. & J. Penfold, T. An on-the-fly deep neural network for simulating time-resolved spectroscopy: predicting the ultrafast ring opening dynamics of 1,2-dithiane. *Phys. Chem. Chem. Phys.* **25**, 13325–13334 (2023).
51. Van Kuiken, B. E. *et al.* Picosecond sulfur K-edge X-ray absorption spectroscopy with applications to excited state proton transfer. *Struct. Dyn.* **4**, 044021 (2017).
52. Cordones, A. A. *et al.* Transient metal-centered states mediate isomerization of a photochromic ruthenium-sulfoxide complex. *Nat Commun* **9**, 1989-1–9 (2018).
53. Kim, Y. *et al.* Ligand-Field Effects in a Ruthenium(II) Polypyridyl Complex Probed by Femtosecond X-ray Absorption Spectroscopy. *J. Phys. Chem. Lett.* **12**, 12165–12172 (2021).
54. Roux, M. V. *et al.* Experimental and Computational Thermochemical Study of Sulfur-Containing Amino Acids: l-Cysteine, l-Cystine, and l-Cysteine-Derived Radicals. S−S, S−H, and C−S Bond Dissociation Enthalpies. *J. Phys. Chem. B* **114**, 10530–10540 (2010).
55. Benson, S. W. Thermochemistry and kinetics of sulfur-containing molecules and radicals. *Chem. Rev.* **78**, 23–35 (1978).
56. Milanesi, L. *et al.* Measurement of energy landscape roughness of folded and unfolded proteins. *Proc. Natl. Acad. Sci.* **109**, 19563–19568 (2012).
57. Kang, H.-S. *et al.* Hard X-ray free-electron laser with femtosecond-scale timing jitter. *Nat. Photonics* **11**, 708–713 (2017).
58. Kim, M., Min, C.-K. & Eom, I. Laser systems for time-resolved experiments at the Pohang Accelerator Laboratory X-ray Free-Electron Laser beamlines. *J. Synchrotron Radiat.* **26**, (2019).
59. Kim, Y. *et al.* Development of an experimental apparatus to observe ultrafast phenomena by tender X-ray absorption spectroscopy at PAL-XFEL. *J. Synchrotron Radiat.* **29**, 194–201 (2022).
60. Møller, Chr. & Plesset, M. S. Note on an Approximation Treatment for Many-Electron Systems. *Phys. Rev.* **46**, 618–622 (1934).
61. Dunning, T. H. Gaussian basis sets for use in correlated molecular calculations. I. The atoms boron through neon and hydrogen. *J. Chem. Phys.* **90**, 1007–1023 (1989).
62. Frisch, M. J. *et al.* Gaussian 16, Revision C.01. (2016).
63. Adamo, C. & Barone, V. Toward reliable density functional methods without adjustable parameters: The PBE0 model. *J. Chem. Phys.* **110**, 6158–6170 (1999).
64. Weigend, F. & Ahlrichs, R. Balanced basis sets of split valence, triple zeta valence and quadruple zeta valence quality for H to Rn: Design and assessment of accuracy. *Phys. Chem. Chem. Phys.* **7**, 3297–3305 (2005).
65. Neese, F. The ORCA program system. *WIREs Comput. Mol. Sci.* **2**, 73–78 (2012).
66. Neese, F. Software update: the ORCA program system, version 4.0. *WIREs Comput. Mol. Sci.* **8**, e1327 (2018).

Acknowledgement

The experiments were carried out using the FXL and CXI instrument at PAL-XFEL (proposal No. 2019-2nd-NCI-032) funded by the Ministry of Science and ICT of Korea. This work was supported by the Global Science Experimental Data Hub Center (GSDC) for data computing and the Korea Research Environment Open NETwork (KREONET) for network service provided by the Korea Institute of Science and Technology Information (KISTI). R. M., J. H. L., D. N. and I. E. were supported by the National Research Foundation of Korea (grant No. 2022M3H4A1A04074153). J.H., N.H. and A.F. acknowledge financial support from the Cluster of Excellence 'CUI: Advanced Imaging of Matter' of the Deutsche Forschungsgemeinschaft (DFG) - EXC 2056 - project ID 390715994. A.F. acknowledges funding from the International Max Planck Graduate School for Ultrafast imaging & Structural Dynamics (IMPRS-UFAST) and from the Christiane-Nüsslein-Vollhard-Foundation. B.Y. acknowledges financial support from the Academy of Medical Sciences Springboard award (SBF006044).

Author contributions

M.O. and N.H. conceived and planned the project. M.O., J.H. and N.H. planned and coordinated the experiments. J.H., R.M., J.H.L., D.N., S.K., I.E., M.K., Y.K., M.G., D.H.H., T.K.K., N.H. executed the experiments. J.H. and N.H. analyzed the experimental data. A.F. performed the theoretical calculations. M.O., J.H., B.Y., and N.H. wrote the manuscript with input from all authors.

Competing interests

The authors declare no competing interests.

Correspondence and requests for materials should be addressed to N. Huse or T.K. Kim. Correspondence concerning spectroscopic modelling should be addressed to A. Freibert.